

# Correlations between multiplicities and average transverse momentum in the percolating colour strings approach

M.A.Braun<sup>a,b</sup>, R.S.Kolevatov<sup>a</sup>, C.Pajares<sup>b</sup> and V.V.Vechernin<sup>a</sup>

<sup>a</sup>)Dep. High-Energy Physics S.Petersburg University, 198504 S.Petersburg, Russia

<sup>b</sup>)Dep. Particle Physics, University of Santiago de Compostela,  
15704 Santiago de Compostela, Spain

## Abstract

Long range correlations multiplicity-multiplicity,  $p_T^2$ -multiplicity and  $p^2 - p_T^2$  are studied in the percolating colour string picture under different assumptions of the dynamics of string interaction. It is found that the strength of these correlations is rather insensitive to these assumptions nor to the geometry of formed fused string clusters. Both multiplicity-multiplicity and  $p_T^2$ -multiplicity correlations are found to scale and depend only on the string density.  $p_T^2$ -multiplicity correlations, which are absent in the independent string picture, are found to be of the order of 10% for central heavy ion collisions and can serve as a clear signature of string fusion. In contrast  $p^2 - p_T^2$  correlations turned out to be inversely proportional to the number of strings and so very small for realistic collisions.

## 1 Introduction

The standard description of particle production in soft high-energy strong interactions is in terms of colour strings stretched between the participant hadrons, whose decay generates the observed particle spectrum. The number of strings grows with energy and atomic number of participants and reaches thousands in heavy ion collision at RHIC and LHC energies. With their density high enough, one expects that the strings begin to overlap and interact. Some time ago a scenario of this interaction was introduced based on the percolation phase transition and existence of colour strings of high colour [1]. An immediate consequence of the percolating string scenario is damping of the multiplicity and rising of the average transverse momentum as compared to the independent string picture. These consequences are in agreement with the first data obtained at RHIC [2]. It is to be stressed that within the percolating string scenario one may imagine different versions of the string interaction dynamics. Overlapping strings may not interact at all. Then the consequence of overlapping

will be just formation of different spots in the interaction area with higher colour content corresponding to the sum of colours of the overlapping strings. These spots will act as independent particle emitters ("overlaps, or "ministrings"). The number of ministrings will generally be much greater than that of initial strings. So in this scenario percolation and fusion of strings actually leads to a proliferation of particle emitters. An opposite scenario with a lot of interaction of overlapping strings assumes that their colour becomes homogeneously distributed over the formed cluster, the latter as a whole becoming an independent particle emitter. In this scenario the number of particle emitters is evidently smaller than the number of initial strings and may become unity if all strings form a single cluster. It is remarkable that these two scenarios actually lead to practically the same predictions for such global quantities as the multiplicity and average transverse momentum. So to distinguish between them one has to study more detailed information about particle spectra. Immediate candidates are the long range correlations between multiplicities or multiplicities and average transverse momentum. In this note we study these observables in both discussed scenarios of string interaction. Our results show that unfortunately these long range correlations are not very sensitive to the choice of string dynamics either. However there is one advantage of studying the long-range correlations involving the average transverse momenta: these correlations are absent in the independent string model. So their presence is a clear signature of string fusion and appearance of spots with higher colour density than on the average. As we shall see, the correlations between the transverse momentum and multiplicity are of especial value, since they depend only on the string density and not on the total number of strings. Long range correlations between transverse momenta, on the contrary, are inversely proportional to the total number of strings and so are practically absent in central heavy ion collisions. They can only be expected to be visible in highly peripheral collisions or collisions involving light nuclei.

Some comments are to be made to explain the application of the colour string approach to correlations. First we shall study long-range correlations, which correspond to choosing the correlating observables from different rapidity windows separated by a reasonably large rapidity interval. This is to exclude short range correlations which are always present and appear both at the string decay stage (internal correlations of string particle production) and final hadronization stage (resonance decays). Second, in the study of average transverse momentum we assume the chosen rapidity windows to exclude the fragmentation regions, where the correlations between the average transverse momentum and multiplicities may largely be a result of summing the transverse momenta of the parent partons from the colliding hadrons. In fact the latter explanation is the standard one for the observed correlations [3]. However it does not apply to the central region, in which particle production becomes insensitive to the parent parton momenta. So hopefully the correlations in the central region result only due to string interactions. Finally we have to remember that the unperturbative colour string picture in the present version is oriented only to soft particle spectra. So our region of average transverse momenta has to be limited by values of the order of  $1 \div 2 \text{ GeV}/c$ .

## 2 General formalism

In this subsection we shall present our basic probabilistic expressions for the correlations valid for any scenario of string interaction.

In a given event colour strings occupy certain regions in the transverse interaction plane and may overlap forming clusters. In any scenario this generates independent emitters, either overlaps or clusters as a whole. We enumerate these emitters by subindex  $\alpha = 1, 2, 3, \dots, M$ , where  $M$  is the total number of emitters.

An event consists of the emission of  $m_\alpha$  particles from emitter  $\alpha$ . The total number of emitted particles is

$$m_e = \sum_{\alpha} m_{\alpha} \quad (1)$$

The  $p_T$  distribution of particles emitted from emitter  $\alpha$  will be given by a certain function  $w_\alpha(p)$ . Note that it corresponds to the average

$$p_\alpha^2 = \int d^2p p^2 w_\alpha(p) \quad (2)$$

whose concrete value depends of the scenario for the interaction. The effective  $p_T$  distribution in a given event is then

$$w_e(p) = \frac{1}{m_e} \sum_{\alpha} m_{\alpha} w_{\alpha}(p) \quad (3)$$

and the average  $p_T^2$  is

$$p_e^2 = \frac{1}{m_e} \sum_{\alpha} m_{\alpha} p_{\alpha}^2 \quad (4)$$

Now we pass to taking averages over many events. This averaging may be divided in two steps. First we average over various events occurring with the same string geometry, that is, with the fixed overlap and cluster structure ("configuration"). Then we have to average over all possible configurations.

To average over events at a fixed configuration we have to know the probability  $\rho_\alpha(m)$  for a given emitter to produce  $m$  particles. This probability has to lead to the average number of particles

$$\bar{m}_\alpha = \sum_m m \rho_\alpha(m) \quad (5)$$

which again is to be taken according to the chosen scenario of string interaction. We get averages in a given configuration:

$$\bar{m}_c = \sum_{\{m_\alpha\}} \prod_{\alpha} \rho_\alpha(m_\alpha) m_e = \sum_{\alpha} \bar{m}_\alpha \quad (6)$$

$$\bar{p}_c^2 = \sum_{\{m_\alpha\}} \prod_{\alpha} \rho_\alpha(m_\alpha) \frac{1}{m_e} \sum_{\alpha} m_\alpha p_\alpha^2 \quad (7)$$

and also the probabilities in a given configuration to emit  $m$  particles

$$\rho_c(m) = \sum_{\{m_\alpha\}} \prod_{\alpha} \rho_\alpha(m_\alpha) \delta_{m, \sum_{\alpha} m_\alpha} \quad (8)$$

and a particle with the transverse momentum  $p$

$$w_c(p) = \sum_{\{m_\alpha\}} \prod_{\alpha} \rho_\alpha(m_\alpha) \frac{\sum_{\alpha} m_\alpha w_\alpha(p)}{\sum_{\alpha} m_\alpha} \quad (9)$$

To study correlations we have to know double distributions. We assume that emissions in the forward and backward rapidity windows are independent. As a result the double distribution in the numbers of particles  $m_F$  and  $m_B$  emitted in the forward and backward rapidity windows in a given configuration factorizes

$$\rho_c(m_F, m_B) = \rho_c^F(m_F) \rho_c^B(m_B) \quad (10)$$

where  $\rho_c^{F,B}(m)$  are given by (8) with emitter probabilities  $\rho_\alpha^{F,B}(m)$  to produce particles in the forward (F) or backward (B) rapidity windows. Similarly the double distribution in the number of particles  $m_F$  in the forward rapidity window and the particle transverse momentum  $p_B$  in the backward rapidity window in a given configuration is a product

$$\rho_c(m_F, p_B) = \rho_c^F(m_F) w_c^B(p_B) \quad (11)$$

Here  $w^B(p)$  is given by (9) with  $\rho_\alpha \rightarrow \rho_\alpha^B$ . Finally the double distribution in momenta  $p_F$  and  $p_B$  of particles emitted in the forward and backward rapidity windows factorizes as

$$w_c(p_F, p_B) = w_c^F(p_F) w_c^B(p_B) \quad (12)$$

To average over different configurations we have to sum these expressions over all configurations with the weight  $P_c$ , which is the probability of a given configuration. We denote this operation as  $\langle \rangle$ . In particular we find various conditional probabilities of interest. The conditional probability to find  $m_B$  particles in the backward rapidity window provided one sees  $m_F$  particles in the forward rapidity window is

$$\langle \rho(m_B) \rangle_{m_F} = \frac{\langle \rho_c(m_F, m_B) \rangle}{\langle \rho_c^F(m_F) \rangle} \quad (13)$$

The conditional probability to find a particle with transverse momentum  $p_B$  in the backward rapidity window provided one sees  $m_F$  particles in the forward rapidity window is

$$\langle w(p_B) \rangle_{m_F} = \frac{\langle \rho_c(m_F, p_B) \rangle}{\langle \rho_c^F(m_F) \rangle} \quad (14)$$

Finally the conditional probability to find a particle with momentum  $p_B$  in the backward rapidity window provided one sees a particle with momentum  $p_F$  in the forward rapidity window is

$$\langle w(p_B) \rangle_{p_F} = \frac{\langle w_c(p_F, p_B) \rangle}{\langle w_c^F(p_F) \rangle} \quad (15)$$

Taking the averages with these probabilities we find our basic formulas for correlations. The average multiplicity in the backward window at a given multiplicity in the forward window is

$$\langle m_B \rangle_{m_F} = \frac{\langle (\bar{m}_B)_c \rho_c^F(m_F) \rangle}{\langle \rho_c^F(m_F) \rangle} \quad (16)$$

where  $(\bar{m}_B)_c$  and  $\rho^F(m_F)$  are given by (6) and (8) for the two rapidity windows. The average transverse momentum squared in some rapidity window at a given multiplicity in a different rapidity window is

$$\langle p_B^2 \rangle_{m_F} = \frac{\langle (p_B^2)_c \rho_c^F(m_F) \rangle}{\langle \rho_c^F(m_F) \rangle} \quad (17)$$

where  $(p_B^2)_c$  is given by (7) with  $\rho_\alpha \rightarrow \rho_\alpha^B$ . Finally the average transverse momentum squared in some rapidity window at a given momentum in a different rapidity window is

$$\langle p_B^2 \rangle_{p_F} = \frac{\langle (p_B^2)_c w_c^F(p_F) \rangle}{\langle w_c^F(p_F) \rangle} \quad (18)$$

where  $w_c^F$  is given by (9) with  $\rho_\alpha \rightarrow \rho_\alpha^F$ . These formulas serve as a starting point for our study.

Expressions for the correlations can be substantially simplified if the emission probabilities  $\rho_\alpha(m)$  have the Poisson form

$$\rho_\alpha(m) = P_{\bar{m}_\alpha}(m) = e^{-\bar{m}_\alpha} \frac{\bar{m}_\alpha^m}{m!} \quad (19)$$

Then taking average in a given configuration can be done analytically.

In particular we find with (19) (see Appendix 1.)

$$\rho_c(m) = P_{\bar{m}_c}(m) = e^{-\bar{m}_c} \frac{\bar{m}_c^m}{m!} \quad (20)$$

$$\bar{p}_c^2 = \frac{1}{\bar{m}_c} \sum_\alpha \bar{m}_\alpha p_\alpha^2 \quad (21)$$

and

$$w_c(p) = \frac{1}{\bar{m}_c} \sum_\alpha \bar{m}_\alpha w_\alpha(p) \quad (22)$$

For particles emitted in the forward (backward) rapidity windows one has to substitute in these formulas  $\bar{m} \rightarrow \bar{m}_{F,B}$

With this simplification, calculation of correlations reduces to taking the averages only over configurations.

### 3 Multiplicity correlations

Forward-backward (FB) correlations between multiplicities has long been studied both experimentally [4] and theoretically [5–7]. On the theoretical level they demonstrate that the number of elementary emitters fluctuates. On this ground they have served as a confirmation of the colour string picture, showing that the number of strings fluctuates, with its average growing with energy. For the FB multiplicity correlations to exist, the interaction between strings is irrelevant: the correlations are fully present when strings are independent. Moreover, as conjectured in [8], interaction and fusion of strings lead to damping of these correlations, since the effective number of strings diminishes. As we shall see this conjecture is confirmed by calculations using Eq. (16) in any of the two scenarios for the string interaction.

### 3.1 Ministrings as emitters

As mentioned in the Introduction the two scenarios differ in the intensity of the interaction between the overlapping strings. The ministring scenario assumes that this interaction is in fact absent: the overlap regions retain their form and serve as independent emitters of particle with characteristics determined by the total colour accumulated in the overlap. In this scenario different emitters can be labeled by two numbers  $\alpha = \{ni\}$  where  $i = 1, 2, \dots$  enumerates overlaps of  $n$  strings. The basic quantity which characterizes the ministring scenario is the average multiplicity of overlap  $\{ni\}$  [4,5]:

$$\bar{m}_{ni} = \mu_0 \sqrt{n} \frac{S_{ni}}{\sigma_0} \quad (23)$$

Here  $S_{ni}$  and  $\sigma_0$  are transverse areas of the overlap and initial string respectively. Using (23) we obtain the average multiplicity in a given configuration as

$$\bar{m}_c = \mu_0 \sum_n \sqrt{n} \frac{S_n}{\sigma_0} \quad (24)$$

where  $S_n = \sum_i S_{ni}$  is the total area in which  $n$  strings overlap and  $\mu_0$  is the average multiplicity for the initial string. The average multiplicities in the forward and backward rapidity windows are given by the same formula with  $\mu_0 \rightarrow \mu_0^{F,B}$ , the forward and backward multiplicities for the initial string:

$$\bar{m}_c^{F,B} = \mu_0^{F,B} \sum_n \sqrt{n} \frac{S_n}{\sigma_0} \quad (25)$$

Putting (25) into (20) and using (16) we reduce calculation of the FB multiplicity correlations to averaging over the overlap geometries of the known expression depending on  $S_n$ . This averaging involves, first, different ways in which string overlap with their total  $N$  number fixed and, second, different values of  $N$  distributed around a certain average value  $\langle N \rangle$  determined by the energy and atomic number of participants. At large  $\langle N \rangle$  and small  $\sigma_0$  as compared to the total interaction area  $S$  one expects a scaling behaviour: appropriately chosen characteristics of the correlations depend only on the dimensionless percolation parameter

$$\eta = \frac{\langle N \rangle \sigma_0}{S} \quad (26)$$

This property allows to study the correlations by Monte-carlo simulations with comparatively low values of  $\langle N \rangle$ . Values of  $\eta$  and  $\langle N \rangle$  for S-S and Pb-Pb central collisions at different energies obtained by Monte Carlo simulations based on the fusing colour string model [1] are shown in Table 1.

In our numerical calculations we studied the quantity

$$F_{\mu-\mu} = \frac{\langle m_B \rangle_{m^F}}{\langle m_B \rangle} - 1 \quad (27)$$

as a function of

$$x = \frac{m_F}{\langle m_F \rangle} \quad (28)$$

In our simulations we used both the homogeneous distribution of strings in the transverse interaction area and the inhomogeneous one, which follows the nuclear profile function  $T(b)$ . No significant qualitative difference was found between these two choices. For simplicity we present here our results for the homogeneous distribution. We chose  $\mu_0^{F,B} = 1$ . We used the Poisson distribution in the number of strings  $N$  with  $\langle N \rangle = 25$  and  $50$ . We have checked that the results are practically independent of  $\langle N \rangle$  in the region  $0.3 < x < 3$ , so that  $F_{\mu-\mu}(x)$  exhibits the expected scaling behaviour for physically relevant values of  $m_F$ .

Our results for values of  $\eta = 0.5 \div 3$  show that in the whole interval  $0 < x < 3$   $F_{\mu-\mu}(x)$  is a monotonously rising function of  $x$ , rather close to linear and crossing zero at  $x = 1$ . Its slope at  $x = 1$  (and  $\langle N \rangle = 50$ ) (the "correlation coefficient")

$$b_{\mu-\mu} = \left( \frac{dF_{\mu-\mu}(x)}{dx} \right)_{x=1}$$

is shown in Fig. 1 by a solid line. As we observe it steadily falls with  $\eta$ , in full accordance with the idea that the correlations diminish as a consequence of string fusion. At very high  $\eta$  the slope seems to flatten against the value around 0.1. At  $\eta \rightarrow 0$  the slope tends to the value 0.5, which corresponds to the independent string model with the assumed value of  $\mu_0$  (see Appendix 1). Note that  $\eta \sim 1.12$  corresponds to the critical value for the percolation phase transition. However our curves do not show any peculiarity at such values of  $\eta$ .

In Fig. 2 we compare  $b_{\mu-\mu}$  for the homogeneous distribution of strings and the inhomogeneous one which follows the nuclear profile function  $T(b) \propto \sqrt{R_A^2 - b^2}$  (corresponding to a constant nuclear density). As mentioned, the difference is of no practical importance.

### 3.2 Clusters as emitters

An alternative scenario with a strong interaction between overlapping strings assumes that the colour becomes homogeneously distributed over the whole cluster formed by the overlapping strings. The emitters are now clusters themselves and index  $\alpha$  now labels just different clusters. The average multiplicity of a cluster is chosen to adjust to the colour distribution [9]:

$$\bar{m}_\alpha = \mu_0 \sqrt{\frac{n_\alpha S_\alpha}{\sigma_0}} \quad (29)$$

where  $n_\alpha$  and  $S_\alpha$  are the number of strings and area of cluster  $\alpha$ . For the forward and backward rapidity window (29) transforms into

$$\bar{m}_\alpha^{F,B} = \mu_0^{F,B} \sqrt{\frac{n_\alpha S_\alpha}{\sigma_0}} \quad (30)$$

Eqs. (29) and (30) express the physical contents of the cluster scenario for multiplicity correlations and their difference from Eqs. (24) and (25) shows the effect of the strong interaction between overlapping strings. The remaining procedure to calculate the correlations does not change as compared to the ministring case.

We calculated the same function  $F_{\mu-\mu}(x)$  (Eq. (29)) with (32) by Monte Carlo simulations. Comparison of our results for  $\langle N \rangle = 25$  and  $50$  again showed a satisfactory scaling

in  $\langle N \rangle$  for  $x = 0.3 \div 3$  and a weak dependence on the way the strings are distributed in the interaction area. In spite of a very different dynamics, we have found no appreciable difference with the former case of overlaps as emitters. The slopes  $b_{\mu-\mu}$  of  $F_{\mu-\mu}(x)$  at  $x = 1$  are shown in Fig. 1 by a long-dashed line (again for  $\langle N \rangle = 50$ ). They are systematically higher than for overlaps but the difference does not exceed 10%, which is of no practical importance, taking into account simplifications involved at the basis of the model.

### 3.3 Fixed number of emitters

Technically taking the average over all geometrical distributions of strings in the transverse area is a formidable task, which can be realistically achieved by Monte Carlo simulations for a reasonable time only for a limited number of strings, substantially smaller than this number in heavy-ion collisions at RHIC and especially LHC energies. On the other hand, it is well-known that different ways of averaging often lead to the same or practically the same averages, since the physical picture of fluctuating variables is often basically the same. This motivates searching for a simplified picture of string fusion, which, on the one hand, is not very different from the discussed above by its physical implications and, on the other hand, avoids geometrical averaging. In this subsection we propose such a picture.

Physically the basis of string fusion model consists of appearance of various emitters homogeneously distributed in the transverse plane with the number of overlapping strings varying for 1 to  $N$  with a certain probability. One can model this physical situation by assuming a fixed number  $M$  of emitters "cells"), each one of them (emitter  $\alpha$ ) equivalent to a certain number  $n_\alpha$  of completely overlapped strings including  $n_\alpha = 0$ , in which case there is no emission at all. So effectively one also has a varying number of emitters with different colours. Averaging over configurations is achieved by distributing each  $n_\alpha$  around some average value  $\bar{n}_\alpha$  with a certain probability  $P_\alpha(n_\alpha)$ . The homogeneous distribution of strings in the transverse plane corresponds to equal averages:  $\bar{n}_\alpha = \bar{n}$ . One can model an inhomogeneous distribution of strings by distributing the  $M$  emitters in the transverse plane and choosing  $\bar{n}_\alpha$  in accordance with the nuclear profile density.

In this model ("cell model" [10]) we have for the average number of particles from cell  $\alpha$

$$\bar{m}_\alpha = \mu_0 \sqrt{n_\alpha}, \quad \bar{m}_\alpha^{F,B} = \mu_0^{F,B} \sqrt{n_\alpha} \quad (31)$$

If we assume that the cell probabilities  $\rho_\alpha(m)$  are Poissonian then correlations can be calculated using our formulas of Section 2 in exactly the same way as before. For the final averaging over configurations (that is over all  $n_\alpha$ ,  $\alpha = 1, \dots, M$ ) we have taken the probabilities  $P_\alpha(n_\alpha)$  to be also Poissonian with a common average value  $\bar{n} = \eta$  to correspond to the previous geometrical picture. Note that in this model the average value of strings is  $\langle N \rangle = M\eta$ .

The results of calculations of  $F_{\mu-\mu}(x)$  in this model for  $\langle N \rangle = 50$  and various  $\eta$  show that they are very close to both previous models, especially at relatively large  $\eta$  when they are nearly identical to those in the ministring picture. The slopes of  $F_{\mu-\mu}(x)$  at  $x = 1$  for the cell model are shown in Fig. 1 with a short-dashed line. So as expected, this simplified model imitates the geometrical model of ministrings almost ideally. With that, it is much simpler: its realization by Monte Carlo simulations requires computer time more than an order of magnitude smaller than for ministrings with equal  $\langle N \rangle$ . Apart from this, the model



admits some analytic estimates for small or large values of  $\eta$ , which reveal basic properties of the correlations in these asymptotical regions (see Appendix 2.).

## 4 Correlations between average transverse momentum and multiplicities

According to Eq. (17) to calculate the correlations  $\langle p_T^2 \rangle - \mu$  we have to know the averages  $\overline{p_c^2}$  in the backward window in a given configuration. For the Poissonian emitters they can be calculated via Eq. (21) if one knows these averages for a given emitter  $\alpha$  (Eq. (2)). The concrete values of  $p_\alpha^2$  depend on the scenario of string interaction. They were analyzed in [8,9] wherefrom we borrow their expressions presented below.

Both for the ministring and cell scenarios the value of  $p_\alpha^2$  for the individual emitter are determined only by the the number of strings in the overlap or cell. For ministrings

$$p_{ni}^2 = p_0^2 \sqrt{n} \quad (32)$$

and for the cell model

$$p_\alpha^2 = p_0^2 \sqrt{n_\alpha} \quad (33)$$

For the cluster scenario  $p_\alpha^2$  depends on the color density inside the cluster and thus also depends on its area  $S_\alpha$ :

$$p_\alpha^2 = p_0^2 \sqrt{\frac{n_\alpha \sigma_0}{S_\alpha}} \quad (34)$$

In these formulas  $p_0^2$  is the average transverse momentum squared for the initial string.

With these expressions for  $p_\alpha^2$  we calculated  $\langle p_B^2 \rangle_{m_F}$  according to Eq. (17) by Monte Carlo simulations for the three scenarios considered: ministrings, clusters and cells. We studied

$$F_{p^2-\mu} = \frac{\langle p_B^2 \rangle_{m_F}}{\langle p_B^2 \rangle} - 1 \quad (35)$$

considered as a function of the same variable  $x$ , Eq.(28). As before we took  $\langle N \rangle = 25$  and 50 and  $\eta$  in the region  $0.5 \div 3$ . We found that  $F_{p^2-\mu}(x)$  again exhibits a satisfactory scaling property: it results practically independent of  $\langle N \rangle$ . As for  $\mu - \mu$  correlations  $F_{p^2-\mu}(x)$  is found to be a nearly linearly rising function of  $x$ , crossing zero at  $x = 1$ . However, contrary to  $\mu - \mu$  correlations, the slopes for  $p^2 - \mu$  correlations rise with  $\eta$ . Slopes of  $F_{p^2-\mu}(x)$  at  $x = 1$

$$b_{p^2-\mu} = \left( \frac{dF_{p^2-\mu}(x)}{dx} \right)_{x=1}$$

are shown in Fig. 3 for the three studied scenarios with the homogeneous distribution of strings. One observes that the overlap and cluster scenarios again lead to practically identical results. The cell model imitates these two physical scenarios quite satisfactory at large  $\eta > 2 \div 2.5$ . At smaller  $\eta$  its slopes lie 30÷40% below. At large  $\eta$  slopes in all three models seem to converge around 0.1. It is remarkable that this value coincides with the corresponding limit for the slopes in  $\mu - \mu$  correlations (cf. Fig. 1). At  $\eta \rightarrow 0$  all slopes vanish, which corresponds to absence of  $p^2 - \mu$  correlations for independent strings.

In Fig. 4 we compare the slopes in the overlap scenario for the homogeneous distribution of strings and the same realistic one, as in Fig. 2. Again the difference results of little importance.

It has to be stressed that absolute values of the slopes are not too small, of the order of 0.1 in a wide range of  $\eta$ . Such slopes can hopefully be measured experimentally. Their existence would be a clear signature of string fusion.

## 5 $p_B - p_F$ correlations

The last type of correlations we shall study are those between transverse momenta of particles emitted in the forward and backward rapidity windows. They can be measured by the average transverse momenta squared of particles in the backward rapidity window at an observed transverse momentum in the forward rapidity window, Eq. (18). To calculate this in our colour string model we have to know the particle spectrum  $w_\alpha(p)$  for an individual emitter. This spectrum has to be chosen to lead to the averages (2), which have been discussed for each of the models for string interaction in the previous section. We choose the distribution  $w_\alpha(p)$  in the form prompted by the standard fit to the experimental spectrum for the proton target [11]

$$w_\alpha(p) = \frac{(\kappa - 1)(\kappa - 2)}{2\pi p_\alpha^2} \left( \frac{p_\alpha}{p + p_\alpha} \right)^\kappa \quad (36)$$

Here  $p_\alpha^2$  is given by Eqs. (32)-(34) for the three models of string interaction considered,  $p_\alpha = \sqrt{p_\alpha^2}$ ,

$$\kappa = 19.7 - 0.86 \ln E, \quad p_0^2 = \frac{24}{(\kappa - 3)(\kappa - 4)} \quad (\text{GeV}/c)^2 \quad (37)$$

and  $E$  is the c.m. energy in GeV.

With this distribution we calculated (18) for the three considered scenarios averaging over configurations by Monte Carlo simulations with different average number of strings  $\langle N \rangle = 25$  and 50. Calculations show that for these correlations the scaling function independent of  $\langle N \rangle$  turns out to be

$$F_{p-p} = \langle N \rangle \frac{\langle p_B^2 \rangle_{p_F}}{\langle p_B^2 \rangle} - 1 \quad (38)$$

As argument it is convenient to choose dimensionless

$$y = \frac{p_F}{\sqrt{\langle p_F^2 \rangle}} \quad (39)$$

We have calculated  $F_{p-p}(y)$  for the for different  $\eta$ . In all cases  $F_{p-p}(y)$  is found to be a linearly rising function of  $y$  crossing zero at  $y = 1$ . The slopes of  $F_{p-p}(y)$  at  $y = 1$

$$b_{p-p} = \left( \frac{dF_{p-p}(y)}{dy} \right)_{y=1}$$

are shown in Fig. 5 as functions of  $\eta$  for the three studied models. They rise with  $\eta$  similarly to the slopes in  $p^2 - \mu$  correlations. Again overlaps and clusters lead to practically identically results. Their imitation by cells gives rather satisfactory results, especially at  $\eta > 2$  where the cell slopes lie higher than those from the other two scenarios by some 10%. At lower  $\eta$  this difference rises to 30÷40 %.

Note that the presence of the factor  $\langle N \rangle$  in (38) together with the calculated values of the scaling function show that for realistic collisions with high enough values of  $\eta$  the magnitude of the correlations is extremely small, which excludes their experimental observation. As follows from our results the correlations can be observed in practice up to  $\langle N \rangle = 10 \div 15$ , which is unrealistic for  $\eta > 1$ .

## 6 Conclusions

This work was primarily motivated by search of appropriate observables which could shed light on the details of dynamics of colour string fusion conjectured to occur in heavy-ion collisions. The results of our study show that pair correlations are unfortunately rather insensitive to these details. Moreover they demonstrate that even the geometric picture of string fusion and percolation is not very essential for the found correlations. A very simplified picture, which only takes into account existence of many emitters with different colours, leads to results not very different from the realistic geometrical overlapping of colour strings. So the correlations basically reflect only the possibility of spots with higher colour field in the colliding nuclei and strongly depend only on their spatial density characterized by the parameter  $\eta$ .

From a certain point of view this is a positive aspect, since predictions for the correlations do not vary with specific assumptions made about the string fusion dynamics. The behaviour of the correlations with  $\eta$  emerges as a clear signature for the basic new phenomenon characteristic for string fusion: formation of emitters with higher colour density. Both  $\mu - \mu$  and  $p^2 - \mu$  correlations look quite promising from this point of view. In particular  $p^2 - \mu$  correlations arise totally due to string fusion in our picture; they are absent with independent strings. However, as mentioned in the Introduction, this is only true for particles produced strictly in the central region, since in the fragmentation regions obvious  $p^2 - \mu$  correlations are caused by the accumulation of the string ends momenta. So to see the effect of string fusion one should choose both rapidity windows as far as possible from the rapidity limits. As to  $p - p$  correlations, our calculations have shown that they diminish with the number of strings and appear to be negligible for realistic heavy-ion collisions except at the highly peripheral collisions.

Our calculations have been made for a homogeneous distribution of strings in the transverse interaction plane. Calculations for a realistic distribution, taking into account the varying string density as a function of impact parameter, are now in progress. However the found insensitiveness of our results to the details of geometry allows to expect that the change introduced by a realistic geometry will be not very essential.

## 7 Acknowledgments

The authors are deeply thankful to Drs. G.A.Feofilov and E.G.Ferreiro for a keen interest in this work and helpful discussions. This work was supported by the RFFI (Russia) grant 01-02-17137 and contract FPA 2002- 01161 of CICYT (Spain)

## 8 Appendix 1. Averages with the Poisson distribution

We start with  $\rho_c(m)$  determined by (8). Presenting the Kronecker symbol as a contour integral around the origin we find

$$\rho_c(m) = \sum_{\{m_\alpha\}} \int \frac{dz}{2\pi iz} z^{-m+\sum_\alpha m_\alpha} \prod_\alpha \rho_\alpha(m_\alpha) \quad (40)$$

We have

$$\sum_{m_\alpha} z^{m_\alpha} P(m_\alpha) = e^{(z-1)\bar{m}_\alpha} \quad (41)$$

so that

$$\rho_c(m) = \int \frac{dz}{2\pi z^{m+1}} e^{(z-1)\bar{m}_c} = e^{-\bar{m}_c} \frac{\bar{m}_c^m}{m!} \quad (42)$$

So we find (20).

Now take average (7). We present it as

$$\bar{p}_c^2 = \sum_m \frac{1}{m} \sum_{\{m_\alpha\}} \prod_\alpha \rho_\alpha(m_\alpha) \delta_{m, \sum_\alpha m_\alpha} \sum_\alpha m_\alpha p_\alpha^2 \quad (43)$$

The internal sum over all  $m_\alpha$  at their sum fixed can be represented in the same way as (40):

$$X \equiv \sum_{\{m_\alpha\}} \int \frac{dz}{2\pi iz} z^{-m+\sum_\alpha m_\alpha} \prod_\alpha \rho_\alpha(m_\alpha) \sum_\alpha m_\alpha p_\alpha^2 \quad (44)$$

Take some particular term in the last sum, say  $\alpha = 1$  Then sums over all  $m_\alpha$ ,  $\alpha = 2, 3, \dots, M$  will give the same factor (41). The sum over  $m_1$  will however contain an extra factor  $m_1$ :

$$\sum_{m_1} z^{m_1} m_1 P(m_1) = e^{(z-1)\bar{m}_1} = z\bar{m}_1 e^{(z-1)\bar{m}_1} \quad (45)$$

So we find

$$X = \sum_\alpha \bar{m}_\alpha p_\alpha^2 e^{-\bar{m}_c} \int \frac{dz}{z^{m_1}} e^{z\bar{m}_c} = \frac{m}{\bar{m}_c} \rho_c(m) \sum_\alpha \bar{m}_\alpha p_\alpha^2 \quad (46)$$

where  $\rho_c(m)$  is given by (20). Putting this into (43) we find that the factor  $m$  in (46) cancels the denominator in (43). Using then

$$\sum_m \rho(m) = 1$$

we find (21).

Derivation of (22) is done in exactly the same way.

## 9 Appendix 2. Analytic estimates in the cell scenario

As mentioned, the cell scenario admits explicit analytic estimates [10] valid in the limit of large or small values of  $\eta$ .

Estimates at large  $\eta$  are based on the asymptotic equivalence of the discrete Poisson distribution and continuous Gaussian distribution

$$P_{\bar{n}}(n) \sim G_{\bar{n}}(n) = \frac{1}{\sqrt{2\pi\bar{n}}} e^{-\frac{(n-\bar{n})^2}{2\bar{n}}} \quad (47)$$

valid in the limit  $\bar{n} \gg 1$ .

Let us first study the simplest case of independent strings (without fusion). Then Eqs. (31) and (33) are changed to

$$\bar{m}_\alpha = \mu_0 n_\alpha, \quad p_\alpha^2 = p_0^2 \quad (48)$$

and similarly for averages in the two rapidity windows. To simplify in this Appendix we shall take  $\mu_0^F = \mu_0^B$  and denote this common multiplicity by  $\mu_0$ . From the second of Eqs. (48) it follows that there will be no  $p^2 - \mu$  correlations as expected. The configuration averages  $\bar{m}_c^{F,B} = \mu_0 \sum_\alpha n_\alpha = \mu_0 N_c$  will depend only on the total number of strings  $N_c$  in a given configuration. Averaging over configuration will be reduced to averaging over the number of strings in different configurations. If the number of strings in each cell is distributed according to the Poisson distribution with average  $\eta$  then the total number of strings will also be distributed according to the Poisson distribution with the average  $M\eta$  (see Appendix 1). So at fixed  $\eta$  the overall average number of strings is related to  $M$  as

$$\langle N \rangle = M\eta \quad (49)$$

Thus, substituting the two Poisson distributions by Gaussians we find from (16)

$$\langle m_B \rangle_{m_F} = \mu_0 \frac{\int_0^\infty N dN N^{-1/2} e^{-\phi(N, m_F)}}{\int_0^\infty dN N^{-1/2} e^{-\phi(N, m_F)}} \quad (50)$$

where

$$\phi(N, m_F) = \frac{(N - \langle N \rangle)^2}{2\langle N \rangle} + \frac{(m_F - \mu_0 N)^2}{2\mu_0 N} \quad (51)$$

We estimate the two integrals by the saddle point method. Then we find

$$\langle m_B \rangle_{m_F} = \mu_0 N_0(m_F) \quad (52)$$

where  $N_0$  is the solution of the equation  $d\phi/dN = 0$ . In terms of scaling quantities

$$x = \frac{m_F}{\langle m_F \rangle}, \quad z = \frac{N}{\langle N \rangle} \quad (53)$$

the equation for the saddle point takes the form

$$z^3 - z^2 = \frac{1}{2}\mu_0(x^2 - z^2) \quad (54)$$

Solving this equation for  $z_0(x)$  one can find function  $\langle m_B \rangle_{m_F}(m_F)$  at all  $m_F$ . The correlation coefficient  $b_{\mu-\mu}$  can however be determined explicitly from (54):

$$b_{\mu-\mu} = \left( \frac{dz}{dx} \right)_{x=1} = \frac{\mu_0}{\mu_0 + 1} \quad (55)$$

Taking  $\mu_0 = 1$  we have  $b_{\mu=\mu} = 0.5$  in full agreement with the limit of curves shown in Fig. 1 at  $\eta \rightarrow 0$ , which corresponds to independent strings.

Now we pass to a physically more interesting case when strings fuse, which in the cell scenario corresponds to Eqs. (31) and (33). Introducing a quantity for a given configuration

$$r_c = \sum_{\alpha} \sqrt{n_{\alpha}} \quad (56)$$

we find

$$\bar{m}_c = \mu_0 r_c, \quad \bar{p}_c^2 = p_0^2 \frac{N_c}{r_c} \quad (57)$$

so that

$$\langle m_B \rangle_{m_F} = \mu_0 \frac{\langle r P_{\mu_0 r_c}(m_f) \rangle}{\langle P_{\mu_0 r}(m_f) \rangle} \quad (58)$$

and

$$\langle p_B^2 \rangle_{m_F} = p_0^2 \frac{\langle (N_c/r_c) P_{\mu_0 r}(m_f) \rangle}{\langle P_{\mu_0 r}(m_f) \rangle} \quad (59)$$

The average is taken over the product of Poisson distributions in  $n_{\alpha}$  each with with the average  $\eta$ .

We consider  $\eta \gg 1$  and substitute all Poisson distributions with Gaussian ones to get

$$\langle m_B \rangle_{m_F} = \mu_0 \frac{\int_0^{\infty} \prod_{\alpha} dn_{\alpha} r_c r_c^{-1/2} e^{-\phi(n_{\alpha}, m_F)}}{\int_0^{\infty} \prod_{\alpha} dn_{\alpha} r_c^{-1/2} e^{-\phi(n_{\alpha}, m_F)}} \quad (60)$$

and

$$\langle p_B^2 \rangle_{m_F} = p_0^2 \frac{\int_0^{\infty} \prod_{\alpha} dn_{\alpha} (N_c/r_c) r_c^{-1/2} e^{-\phi(n_{\alpha}, m_F)}}{\int_0^{\infty} \prod_{\alpha} dn_{\alpha} r_c^{-1/2} e^{-\phi(n_{\alpha}, m_F)}} \quad (61)$$

where

$$\phi(n_{\alpha}, m_F) = \sum_{\alpha} \frac{(n_{\alpha} - \eta)^2}{2\eta} + \frac{(m_F - \mu_0 r_c)^2}{2\mu_0 r_c} \quad (62)$$

In the saddle point approximation we find

$$\langle m_B \rangle_{m_F} = \mu_0 r_0, \quad \langle p_B^2 \rangle_{m_F} = p_0^2 \frac{N_0}{r_0} \quad (63)$$

where  $N_0$  and  $r_0$  are values of  $N_c$  and  $r_c$  at the saddle point defined by the equations

$$\frac{\partial \phi(n_{\alpha}, m_F)}{\partial n_{\alpha}} = 0, \quad \alpha = 1, \dots, M \quad (64)$$

Introducing scaled variables

$$x = \frac{m_F}{\langle m_F \rangle}, \quad z_\alpha = \sqrt{\frac{n_\alpha}{\eta}}, \quad (65)$$

and a constant involving  $\eta$

$$a = \frac{\mu_0}{4\sqrt{\eta}} \quad (66)$$

we can write the saddle point equations in the form

$$z_\alpha^3 - z_\alpha = a \left( x^2 \frac{M^2 \eta}{r_c^2} - 1 \right), \quad \alpha = 1, \dots, M \quad (67)$$

In terms of  $z_\alpha$  here  $r_c = \sqrt{\eta} \sum_\alpha z_\alpha$ . Due to symmetry in  $\alpha$  obviously for the solution  $z_\alpha = z$  where  $z$  satisfies a single equation

$$z^3 - z = a \left( \frac{x^2}{z^2} - 1 \right) \quad (68)$$

This equation defines  $z = z(x)$ , in terms of which one finds

$$F_{\mu-\mu}(x) = F_{p^2-\mu} = z(x) - 1 \quad (69)$$

So at large values of  $\eta$  both  $\mu - \mu$  and  $p^2 - \mu$  correlations are described by the same scaling function of  $x$ .

At  $x = 1$  Eq. (68) possesses an obvious trivial solution:

$$x = 1, \quad z = 1, \quad r_0 = M\sqrt{\eta}, // N_0 = \langle N \rangle = \mu_0 M \quad (70)$$

This is sufficient to calculate the (identical) correlation coefficients for both  $\mu - \mu$  and  $p^2 - \mu$  correlations:

$$b_{\mu-\mu} = b_{p^2-\mu} = \frac{\mu_0}{\mu_0 + 4\sqrt{\eta}} \quad (71)$$

It slowly falls with  $\eta$  Of course one should have in mind that these are only asymptotic estimates, valid at sufficiently high  $\eta$ . To see their validity region we present in Fig. 6 the slopes  $b$  in  $\mu - \mu$  and  $p^2 - \mu$  correlations as functions of  $\eta$  with  $\mu_0 = 1$  calculated by Monte-Carlo simulations, together with the common asymptotic curve (71). As one observes the asymptotic curve gets more or less close to the exact ones starting from  $\eta > 4 \div 5$ . These are very high values from the physical point of view, attainable only at energies in the multi-TeV region for the heaviest nuclei and central collisions.

## 10 References

1. M.A.Braun and C.Pajares, Nucl. Phys. **B390**(1993)542,549;  
N.Armento, M.A.Braun, E.G.Ferreiro and C.Pajares, Phys. Rev. Lett. **77** (1996) 3736l  
N.S.Amelin, M.A.Braun and C.Pajares, Phys.Lett. **B 306** (1993) 312l Z.Phys. **C6 63** (1994) 507.

2. M.A.Braun, F.del Moral and C.Pajares, Phys. Rev. **C65** (2002) 024907.
3. A.Capella and A.Krzywicki, Phys. Rev. **D29** (1984) 1007;
- P.Aurenche, F.Bopp and J.Ranft, Phys. Lett. **B147** (1984) 212;
- A.Capella, J.Tran Thanh Van and J.Kwiecinski, Phys. Rev. Lett., **58** (1987) 2015.
4. I.Derado *et al.*, Z.Phys. **c 40** (1988) 25.
5. A.Capella and J. Tran Thanh Van, Phys. Rev., **D 29** (1984) 2512.
6. T.T.Chou and C.N.Yang, Phys. Lett. **B135** (1984) 175; Phys. Rev., **D 32** (1985) 1692.
- M.A.Braun, C.Pajares and V.V.Vechernin, Phys. Lett., **B 493** (2000) 54.
7. N.S.Amelin, N.Armesto, M.A.Braun, E.G.Ferreiro and C.Pajares, Phys. Rev. Lett. **73** (1994) 2813
8. M.A.Braun and C.Pajares, Eur. Phys. J. **C16** (2000) 349.
9. M.A.Braun, F.del Moral and C.Pajares, Eur. Phys. J. **C21** (2001) 557.
10. V.V.Vechernin, R.S.Kolevatov, hep-ph/0304295; hep-ph/0305136.
11. M.A.Braun and C.Pajares, Phys. Rev. Lett., **85** (2000) 4864.



## 11 Table

Values of  $\eta$  and average number of strings  $\langle N \rangle$  for central S-S and Pb-Pb collisions at different energies

**S-S scattering ( $b = 0$ )**

$\sqrt{s}$	$\eta$	$\langle N \rangle$
19.4	0.40	126
62.5	0.52	164
200	0.65	204
546	0.80	252
1800	0.97	308
7000	1.23	390

**Pb-Pb scattering ( $b = 0$ )**

$\sqrt{s}$	$\eta$	$N$
19.4	1.08	1190
62.5	1.39	1536
200.0	1.60	1800
546.0	2.03	2240
1800.0	2.46	2720
7000.0	3.03	3350

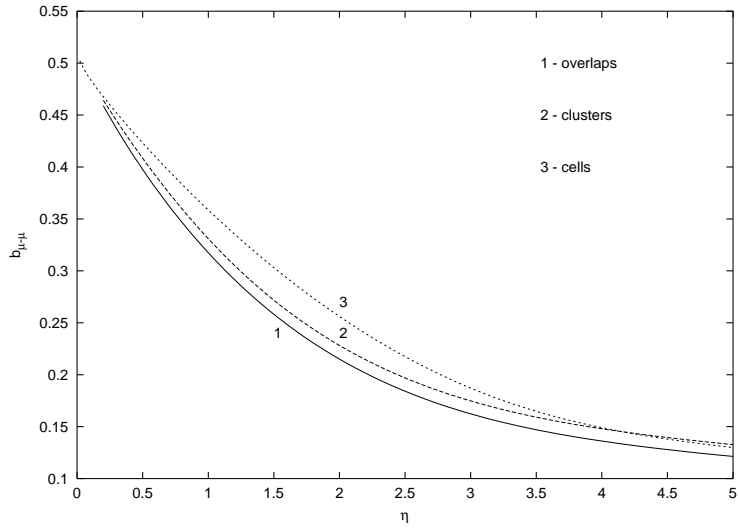


Figure 1: Correlation coefficient  $b$  for  $\mu - \mu$  correlations in the three scenarios studied.

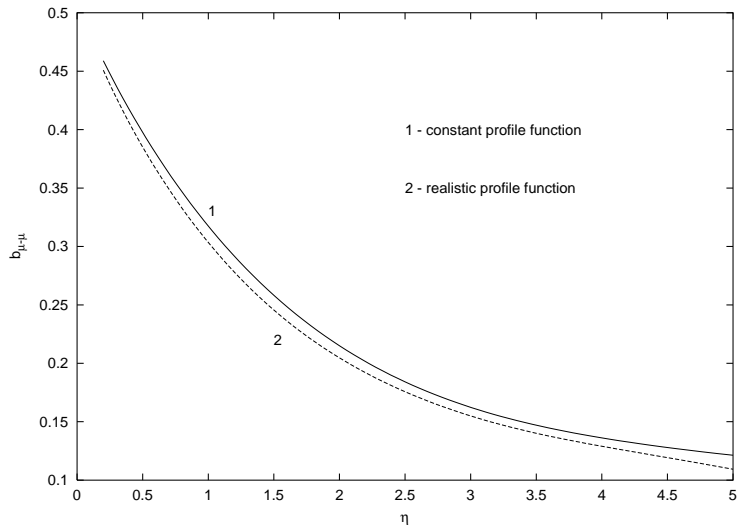


Figure 2: Correlation coefficient  $b$  for  $\mu - \mu$  correlations in the overlap scenario for the homogeneous distribution of strings and the one proportional to  $T(b) \propto \sqrt{R_A^2 - b^2}$ .

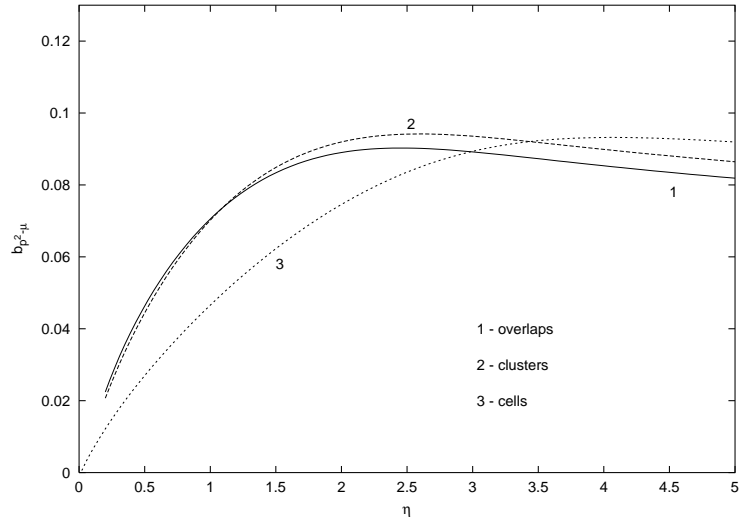


Figure 3: Correlation coefficient  $b$  for  $p^2 - \mu$  correlations in the three scenarios studied.

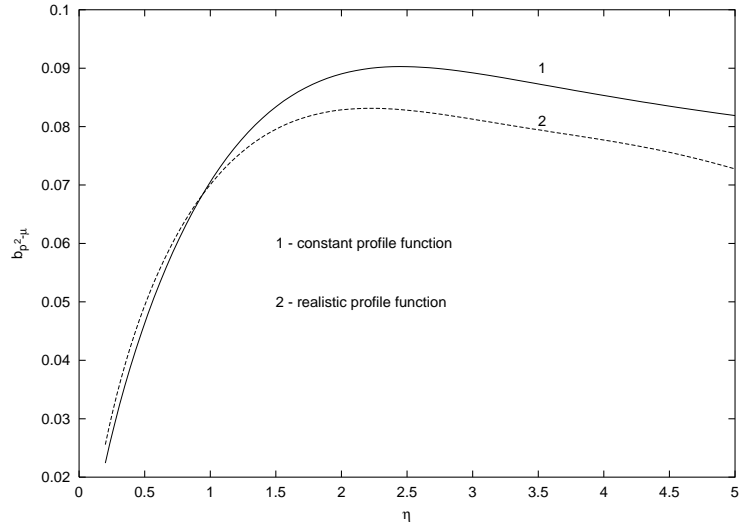


Figure 4: Correlation coefficient  $b$  for  $p^2 - \mu$  correlations in the overlap scenario for the homogeneous distribution of strings and the one proportional to  $T(b) \propto \sqrt{R_A^2 - b^2}$ .

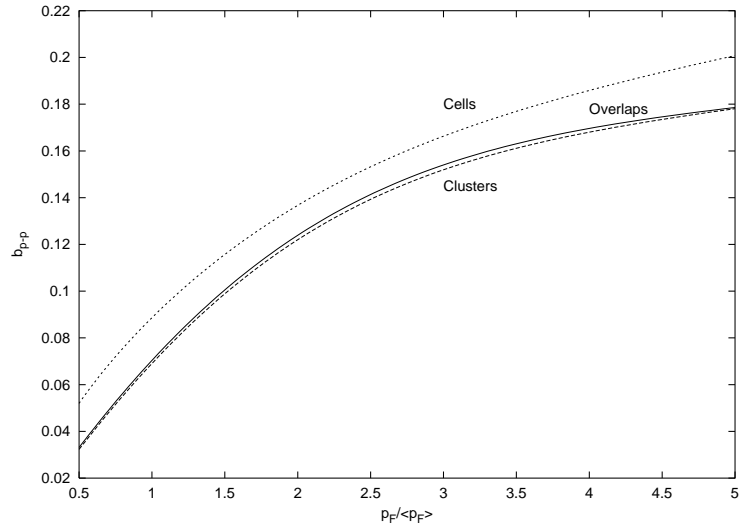


Figure 5: Correlation coefficient  $b$  for  $p - p$  correlations in the three scenarios studied.

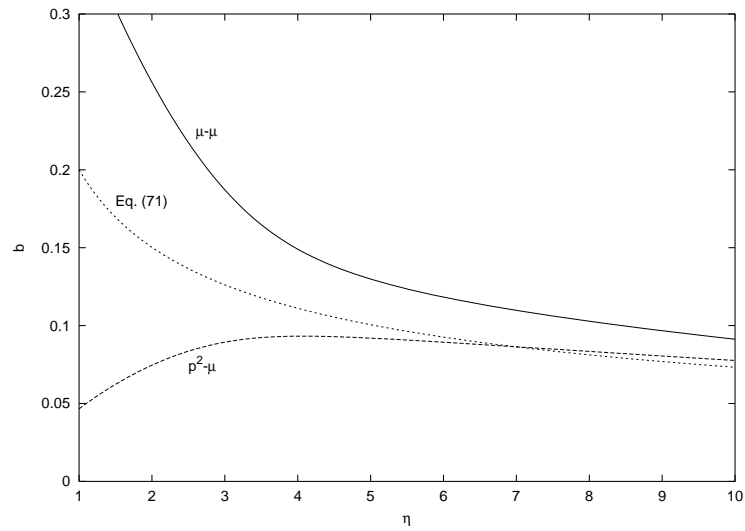


Figure 6: Correlation coefficients for  $\mu - \mu$  and  $p^2 - \mu$  correlations in the cell model together with the asymptotics (71).